Università degli Studi di Bologna

FACOLTÁ DI INGEGNERIA

Corso di Dottorato in
ING-IND/13: MECCANICA APPLICATA ALLE MACCHINE
Ciclo XXI

Spatial mechanisms for modelling the human ankle passive motion

Tesi di Dottorato di:
Ing. Riccardo Franci

Coordinatore:
Chiar.mo Prof. Vincenzo Parenti Castelli

Relatore:
Chiar.mo Prof. Vincenzo Parenti Castelli

Anno Accademico 2008-2009

Contents

Chapter 1

Introduction

The majority of human joints are the diarthrodial joints, also called synovial joints, which allow the main movements of the human body. In particular, the knee and the ankle joints play a fundamental role in human locomotion, thus, the study of human diarthrodial joints involved efforts of an impressive number of researchers. A deeper understanding of the normal behaviour of these joints is still a crucial issue which must be further pursued in order to improve the treatment of joint degeneration, surgical planning and prosthetic design.

Basic studies focussed on experimental measurements of the relative motion of the main bones of the joint under investigation. The measurements performed in *vitro* (cadaver specimens) and/or in *vivo* (patients and volunteers) have the following various purposes:

- to test and validate measurement techniques [1,2] as well as define standardization of diagnosis and rehabilitation procedures;
- to obtain a deeper knowledge on the behaviour of these joints which exhibit a quite complicated anatomical structure [3];
- to validate and improve mathematical models of the articulations [4,5].

Mathematical models are among the most powerful tools for the functional analysis of such a complicated biological structures and represent helpful tools for the solution of important issues such as, for instance:

- definition of surgical and diagnostic procedures for joint disorders caused by injuries and/or diseases;
- designing prosthesis devices [6,7];
- assessment of the role of the joint biological structures in the joint characteristics in normal and pathological conditions [2];

The models presented in the literature are based on two different approaches. The first one models the biological structures of the joint connections such as ligaments, muscles, and articular surfaces by means of linear and non-linear elastic

and dumping elements, lumped and/or distributed parameters, and finds the relative motion of the main bones by solving the equations of motion of the resulting model [1, 8–10]. The main bones are allowed to have up to six degrees of freedom (DOF) in their relative motion which finally depends on the external forces applied to the joint and on the elastic and dumping characteristics of the joint connecting structures. These models are computationally demanding but are also suitable to simulate the dynamic behaviour of the joint in addition to its kinematic and static behaviour. The second approach, instead, models the joint as a linkage or an equivalent mechanism [4, 5, 11] whose geometry is based, as much as possible, on the joint's anatomical structures. The motion of the mechanism predicts the relative motion of the joint's main anatomical structures. These mechanisms (equivalent mechanisms) are suitable to analyze the passive motion of the joint.

The passive motion of a diarthrodial joint, i.e. the relative motion of the main bones of the joint under virtually unloaded conditions, is of great importance [2, 5] to both understand the role of the main anatomical structures of the joint (ligaments, articular surfaces, etc.) and perform a more reliable dynamic analysis. The passive motion, frequently approximated with a planar motion, is indeed a very complex spatial motion.

In particular, as a consequence of the high number of operations and prosthetic replacements, the knee is one of the most studied joints and there are several models of it, both bi-dimensional [3, 7, 12] and three-dimensional [5, 13–15], aimed at replicating the motion of this joint.

Based on a similar approach and by the same motivations, the ankle joint (also known as tiobiotalar joint) has been studied too. One of the first models of the ankle joint was the one-degree-of-freedom (DOF) planar four-bar linkage [3]. More recently, clinical evidence and experimental results showed that the passive relative motion of the tibia and the talus, which are the main bones of the ankle joint, is a complex spatial motion that can be replicated by one-DOF spatial equivalent mechanisms [16]. These mechanisms are based on the geometry of the main anatomical structures of the ankle joint, namely on the shape of the talus and tibio/fibula bones at their interface, and on two main ligaments.

In [16] the relative motion of the talus/calcaneus, considered as a single bone, with respect to the tibia/fibula, also considered as a single bone, was modelled by two different equivalent mechanisms. The first one features three sphere-to-plane contact points between the talus and the tibia/fibula bones, while the second one models the tibiotalar interface by a single spherical pair. Two ligaments were considered in each model which constrained the relative motion of the two main bones to a one-DOF motion. These two models were only partially satisfactory since they did not fully replicate the measured natural ankle joint passive motion.

The aim of this dissertation will focus on the kinematic modeling of the ankle complex joint to contribute for a better understanding of the passive 3D mobility of the tibiotalar joint with the hypothesis that this is obtained by the synergetic role of the ligaments and of the articular surfaces.

To this purpose, two mechanisms are proposed in this dissertation as equivalent

mechanisms which overcome the limitations of the previous models and makes it possible to better replicate the passive motion of the joint.

The geometry of these devised mechanisms relies upon the anatomical structures of the ankle complex; namely, on the talus and tibio/fibular articular surfaces on one side and on some ligaments on the other side.

A new procedure to synthesize the optimal geometry of these mechanisms will be presented and used in an iterative refinement process to provide the final geometry of the mechanism.

In order to show the accuracy of the models and the efficiency of the proposed procedure, these mechanisms are synthesized from experimental data and the results are compared with those obtained both during experimental sessions and with data published in the literature.

Chapter 2

Modelling of the human ankle joint

2.1 Anatomy of the ankle

In this section the fundamental anatomical structures of the ankle joint, the nomenclature and the conventions adopted in this dissertation are presented.

2.1.1 Anatomical structures

The human ankle joint features three main bones: the tibia (T_i) which forms the inside, or medial, portion of the ankle; the fibula (F_i) which forms the lateral, or outside portion of the ankle; and the talus (T_a) underneath (Figure 2.1). Furthermore, the bottom of the talus sits on the heelbone, called the calcaneus (C_a). This two bones of the foot are connected to make the subtalar joint, also known as the talocalcaneal joint. The lateral malleolus of the F_i and the medial malleolus of the T_i along with the inferior surface of the distal T_i articulate with three facets of the T_a.

The ankle joint is formed by several anatomical parts which will be called *structures*, *elements* or *components* in the following, without distinction. They can be divided into passive and active structures. Passive structures are those elements which can exert forces only if externally stressed: articular surfaces, ligaments and other ligamentous structures belong to this category. On the contrary, active structures, such as the muscles, can intrinsically exert forces but, in general, they almost do not oppose external forces when inactive.

In this dissertation only the passive structures are considered. In particular the passive motion of the main bones of the human joints, that is the motion under virtually unloaded conditions, is studied in order to clarify the role played by the principal anatomical structures of the articulation (such as articular surfaces and ligaments). Ligaments are very important ankle joint elements which have a strong influence on the mobility and stability[1] of the joint. Ligaments are the soft tissues

[1] Joint resistance to relative movement of the bones when load is applied

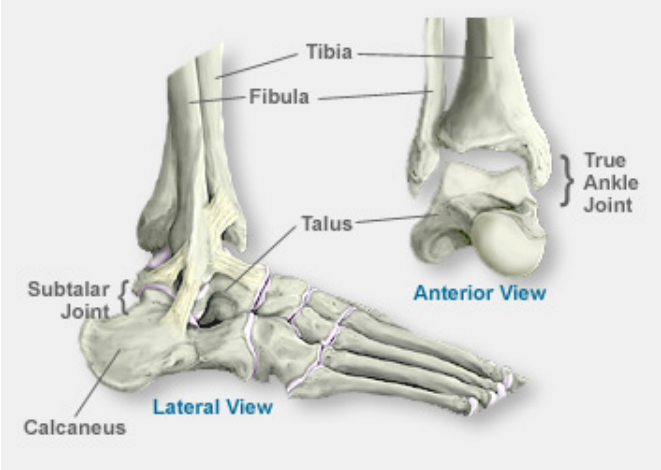

Figure 2.1: Lateral and anterior view of the human ankle bones.

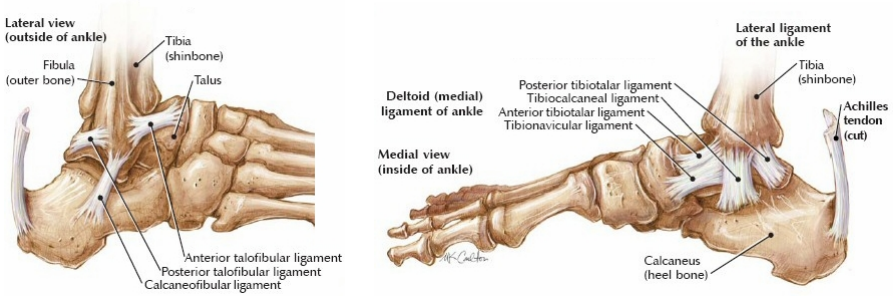

(a) (b)

Figure 2.2: The ligaments of the foot from the (a) lateral and (b) medial aspect [17].

that attach bones to bones. These structures are made up of small fibers of a material called collagen. The collagen fibers are bundled together to form a rope-like structure. Ligaments come in many different sizes and like rope, are made up of many smaller fibers. Thickness of the ligament determines its strength. The most important ligaments of the ankle joint provide a bone-to-bone interconnection between the T_i, F_i, T_a and C_a (Figure 2.2). The connective area between a ligament and a bone will be called *attachment* or *attachment area* in the following, without distinction.

The ligaments of the ankle joint are grouped into two categories, the *lateral collateral* ligaments and the *medial collateral* ligaments. Although the ligaments of the ankle are strong fibrous bands, they are often susceptible to injury due to the excessive movement of the subtalar joint during activity.

The lateral collateral ligaments include the anterior *talofibular* ligament, *calcaneofibular* ligament (CAFiL), *talocalcaneal* ligament, *posterior talocalcaneal*

ligament and the *posterior talofibular* ligament. The anterior talofibular ligament passes from the tip of the lateral malleolus to the T_a anteriorly. The calcaneofibular ligament passes from the lateral malleolus to the C_a with the talocalcaneal ligament running at its base. The posterior talofibular ligament passes from the tip of the lateral malleolus to the T_a posteriorly. The posterior talocalcaneal extends this band to the C_a.

The medial collateral ligaments, or deltoid ligament, include the tibionavicular ligament, *calcaneotibial ligament* (TiCaL), anterior talotibial ligament, and the posterior talotibial ligament. The tibionavicular ligament runs anteriorly form the medial malleolus to the navicular bone. The calcaneotibial ligament runs from the tip of the medial malleolus to the edge of the C_a. The anterior and posterior talotibial ligaments run anteriorly and posteriorly between the medial malleolus and the T_a.

From the intricate ligamentous apparatus which surrounds the ankle joint complex, fibres of the CaFiL and TiCaL were demonstrated to move nearly isometrically throughout the flexion arc [3, 4].

2.1.2 Anatomical planes

In Figure 2.3 the anatomical planes are represented.

- A *transverse* (also known as axial or horizontal) plane is an X-Y plane, parallel to the ground, which (in humans) separates the superior from the inferior, or put another way, the head from the feet.
- A *frontal* (also known as coronal) plane is an X-Z plane, perpendicular to the ground, which (in humans) separates the anterior from the posterior, the front from the back, the ventral from the dorsal.
- A *sagittal* (also known as median) plane is an Y-Z plane, perpendicular to the ground, which separates left from right.

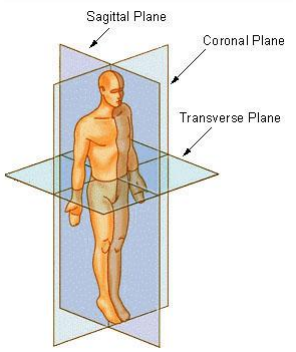

Figure 2.3: Anatomical planes of the human body.

2.2 Ankle joint motion

The relevant literature reports (a) conflicting deductions regarding the number of degrees of freedom (DOF) of the ankle joint and (b) contradictory observations on geometry and pattern of contact of the articular surfaces, and on pattern of slackening/tightening of the ligament fibres [18, 19]. The most recent findings shows that the motion at the articulation between the inferior surface of the T_a and the superior surface of the C_a, i.e. the subtalar joint, is considerable only when deviation forces are applied in the transverse and frontal planes but is very small in passive motion [3, 20]. In the latter condition, large spatial motion occurred at the tibiotalar joint apparently guided by the passive structures alone. Contact occurs at the upper articulations, medial and lateral, of the T_a with the tibial mortise, also between the lateral T_a and the internal distal F_i.

In order to identify every point of the joint, it is necessary to define reference frames. In particular, it is convenient to define the anatomical frames attached to the bones: the coordinates of a point of a bone expressed in the corresponding anatomical frame do not change with ankle joint configuration. Therefore, since the C_a is considered as rigidly joined with the T_a (talocalcaneal segment) and the F_i is considered as rigidly attached to the tibia (tibiofibular segment), the passive motion of the ankle joint can be described by means of two anatomical frame fixed on the tibiofibular (T_i/F_i) segment and talocalcaneal (T_a/C_a) segment respectively.

The relative pose (position and orientation) between two bones can be described by means of the kinematic parameters which define the relative poses of the corresponding reference frames.

In order to define two anatomical frames embedded into the T_i/F_i and T_a/C_a respectively, some anatomical landmarks were digitized.

In particular, the tibia-fibula anatomical reference system (S_f) was defined as follows, according to a known convention [21]:

- origin: located at the midpoint between the tips of the lateral and medial malleoli;

- x-axis: the line perpendicular to the quasi-frontal plane defined by the tips of the malleoli and the head of the F_i, and pointing anteriorly;

- z-axis: the line connecting the tips of the malleoli, and pointing to the right hand side of the body;

- y-axis: orthogonal to the previous two, according to the right hand rule.

Likewise, the talus-calcaneus anatomical reference system (S_c) was defined as follows:

- origin: located at the midpoint between the tips of the posterior ends of the lateral and medial ridges of the trochlea tali;

- y-axis: the line perpendicular to the quasi-transverse plane defined by these posterior tips and the head of the T_a, and pointing proximally;
- x-axis: the line connecting the origin and the head of the T_a, and pointing forward;
- z-axis: orthogonal to the previous two, and pointing to the right according to the right hand rule.

The 4x4 transformation matrices ${}_{F,f}T$, (which transforms homogeneous coordinates from the tibiofibular anatomical system to a reference system of the tracker on T_i) and ${}_{C,c}T$, (which transforms homogeneous coordinates from the talocalcaneal anatomical system to a reference system of the tracker on T_a) were defined. The transformation matrix ${}_{f,c}T$ from S_c to S_f was then computed by the following transformation:

$$ {}_{f,c}T = ({}_{G,f}T)^{-1} \cdot {}_{G,c}T \tag{2.1} $$

where S_G is the reference system fixed to the camera and

$$ \begin{aligned} {}_{G,f}T &= {}_{G,F}T \cdot {}_{F,f}T \\ {}_{G,c}T &= {}_{G,C}T \cdot {}_{C,c}T \end{aligned} \tag{2.2} $$

In order to define the relative orientation of T_a with respect to T_i, a sequence-independent joint coordinate system [22] was adopted. The three following axes were chosen: the y-axis of S_f fixed to the T_i, the z-axis of S_c fixed to the T_a, and a floating axis defined by the cross vector product of the unit vectors of the y-axis of S_c and the unit vector of the z-axis of S_f. Three angles about these axes were defined respectively (Figure 2.4a): angle α, ankle internal(+)/external(-) rotation, angle γ, ankle dorsiflexion(+)/plantarflexion(-), and angle β, ankle pronation(+)/supination(-). Internal and external rotation are also known as adduction and abduction rotation respectively. The range of the plantarflexion and dorsiflexion of the ankle joint is shown in Figure 2.4b.

2.2.1 Ankle joint coordinate systems

The rotation matrix R which transforms the components of a vector from system S_c to system S_f can be expressed as a function of α, β and γ [23, 24].

This section provides the equations used to compute the rotation angles used in this dissertation and applied to the human ankle joint.

As shown in Figure 2.5, the Cartesian systems S_f and S_c are embedded in the T_i and T_a respectively.

Unit vectors of the coordinate system which define the axes are denoted as $\mathbf{e}_1$, $\mathbf{e}_2$ and $\mathbf{e}_3$. The rotation axis $\mathbf{e}_1$, fixed to the T_i, is chosen coincident with the z_f-axis so that the rotation about it corresponds to the clinical motion of dorsi/plantar flexion. The rotation axis $\mathbf{e}_3$, fixed to the T_a, is chosen coincident with the y_c-axis and the rotation about it corresponds to the clinical motion of internal/external

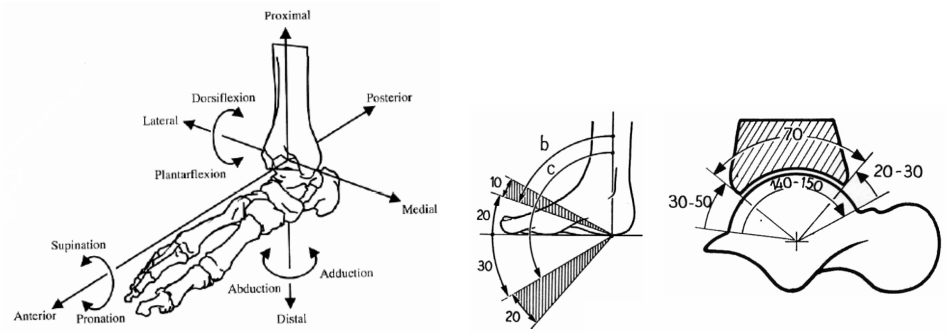

(a) (b)

Figure 2.4: (a) Axes rotation for the right ankle joint; (b) range of the plantar and dorsi flexion angles.

rotation of the foot. The floating axis, defined by the unit vector $\mathbf{e}_2$, is the common perpendicular to the body fixed axes. Therefore, its orientation is given by the cross product of the unit vectors which define the orientation fixed axes:

$$\mathbf{e}_2 = \frac{\mathbf{e}_3 \times \mathbf{e}_1}{\|\mathbf{e}_3 \times \mathbf{e}_1\|} \tag{2.3}$$

The three angular rotations (γ, β, α) about $\mathbf{e}_1$, $\mathbf{e}_2$ and $\mathbf{e}_3$ respectively represent the clinical orientation of the foot with the convention described in Section 2.2.

The rotation matrix, that describes the orientation of S_c to S_f, is conveniently defined by thinking of the ankle joint in neutral position with the coordinate systems parallel to one another. In this configuration the direction of the unit vector $\mathbf{e}_2$ is coincident with the direction of the x-axis. If therefore, R_x, R_y and R_z described the rotation matrices about the axes $\mathbf{e}_2$, $\mathbf{e}_3$ and $\mathbf{e}_1$ respectively they can be expressed as follows:

$$R_{\mathbf{e}_1,\gamma} = \begin{bmatrix} c_\gamma & -s_\gamma & 0 \\ s_\gamma & c_\gamma & 0 \\ 0 & 0 & 1 \end{bmatrix} R_{\mathbf{e}_2,\beta} = \begin{bmatrix} 1 & 0 & 0 \\ 0 & c_\beta & -s_\beta \\ 0 & s_\beta & c_\beta \end{bmatrix} R_{\mathbf{e}_3,\alpha} = \begin{bmatrix} c_\alpha & 0 & s_\alpha \\ 0 & 1 & 0 \\ -s_\alpha & 0 & c_\alpha \end{bmatrix} \tag{2.4}$$

where c_x and s_x stand for $cos(x)$ and $sin(x)$ respectively.

If considering a right (Figure 2.5a) and according to right hand rule, the rotation matrix that describes the orientation of S_c to S_f, is given as rotation about three axes:

$$R_{right} = R_{\mathbf{e}_1,\gamma} \cdot R_{\mathbf{e}_2,-\beta} \cdot R_{\mathbf{e}_3,\alpha} \tag{2.5}$$

$$R_{right} = \begin{bmatrix} c_\alpha c_\gamma + s_\alpha s_\beta s_\gamma & -s_\gamma c_\beta & s_\alpha c_\gamma - c_\alpha s_\beta s_\gamma \\ c_\alpha s_\gamma - s_\alpha s_\beta c_\gamma & c_\gamma c_\beta & s_\alpha s_\gamma + c_\alpha s_\beta c_\gamma \\ -c_\beta s_\alpha & -s_\beta & c_\alpha c_\beta \end{bmatrix} \tag{2.6}$$

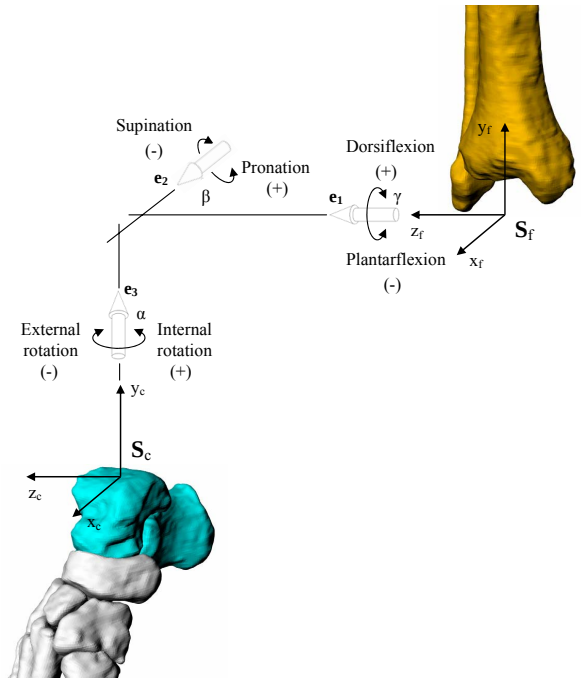

(a)

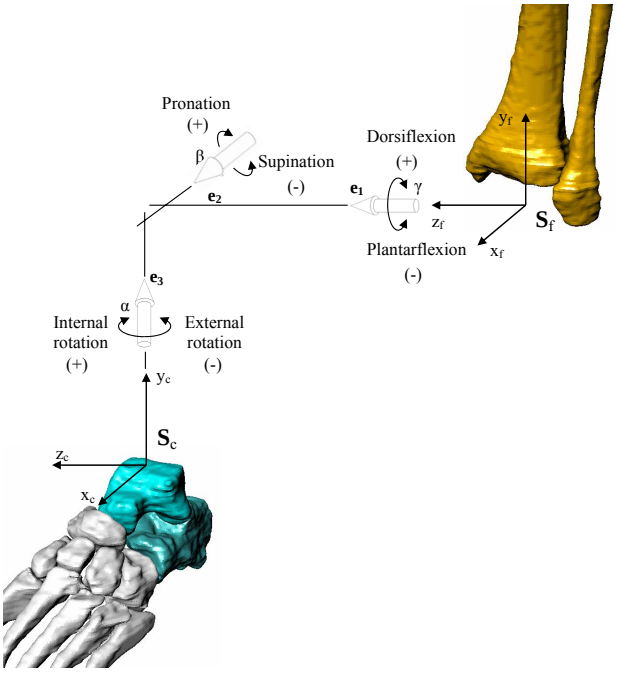

(b)

Figure 2.5: The Joint Coordinate System for the right leg (a) and the left leg (b).

In order to maintain the same clinical meaning for the rotations (α, β, γ) if considering a left leg, the sign of the angles α and β should be opposite to the right leg angles, as shown in Figure 2.5b. Therefore, in this case the rotation matrix that describes the orientation of S_c to S_f, can be computed as:

$$R_{left} = R_{\mathbf{e}_1,\gamma} \cdot R_{\mathbf{e}_2,\beta} \cdot R_{\mathbf{e}_3,-\alpha} \tag{2.7}$$

$$R_{left} = \begin{bmatrix} c_\gamma c_\alpha + s_\gamma s_\beta s_\alpha & -s_\gamma c_\beta & -c_\gamma s_\alpha + s_\gamma s_\beta c_\alpha \\ s_\gamma c_\alpha - c_\gamma s_\beta s_\alpha & c_\gamma c_\beta & -s_\gamma s_\alpha - c_\gamma s_\beta c_\alpha \\ c_\beta s_\alpha & s_\beta & c_\beta c_\alpha \end{bmatrix} \tag{2.8}$$

If the rotation matrix R (R_{right} or R_{left} if the leg is right or left respectively) is known and given by

$$R = \begin{bmatrix} r_{11} & r_{12} & r_{13} \\ r_{21} & r_{22} & r_{23} \\ r_{31} & r_{32} & r_{33} \end{bmatrix} \tag{2.9}$$

the rotation angles (α, β, γ) can be computed as:

$$\begin{aligned} \beta &= atan2\left(r_{3,2}, \pm\sqrt{r_{3,1}^2 + r_{3,3}^2}\right) \\ \alpha &= atan2\left(\frac{-r_{3,1}}{c_\beta}, \frac{r_{3,3}}{c_\beta}\right) \\ \gamma &= atan2\left(\frac{-r_{1,2}}{c_\beta}, \frac{r_{2,2}}{c_\beta}\right) \end{aligned} \tag{2.10}$$

where $atan2(y,x) = arctan\left(\frac{y}{x}\right)$.

2.3 Kinematic models of the equivalent mechanisms

Several studies [3, 4] have shown that during passive joint flexion the ankle complex behaves as a one-DOF mechanism. In particular, the relative movement of the T_i and T_a during passive flexion is a complex motion but single repeatable path constrained by articular surfaces and ligaments: once the flexion angle is imposed to the articulation, the corresponding pose of the T_a with respect to the T_i is defined, both univocally and experimentally replicable. Furthermore, since no forces are applied to the articular components, they are subjected to no deformations, therefore the passive motion of the ankle can be modelled by means of a rigid link mechanism; the relative motion of the T_i and T_a can thus be obtained from the kinematic analysis of the equivalent mechanism. In the following sections will be presented two equivalent mechanisms of the ankle joint.

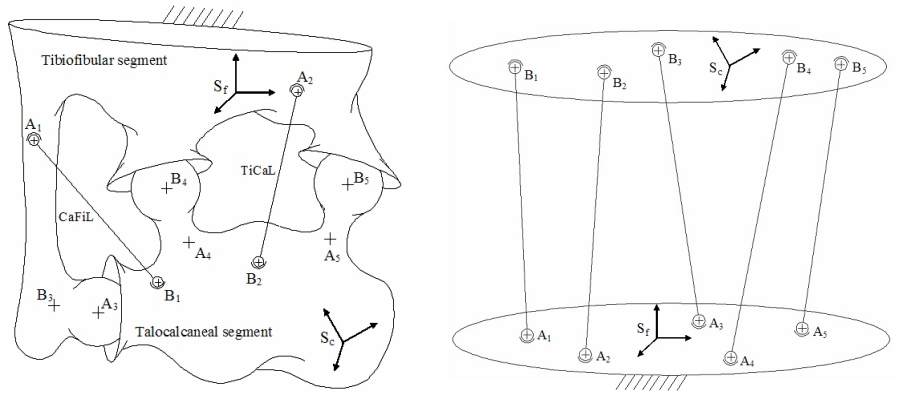

Figure 2.6: (a) Schematic of the ankle complex joint; (b) the 5-5 fully-parallel mechanism.

2.3.1 The 5-5 fully parallel mechanism

Based on a careful inspection of the tibiocalcaneal interface, the T_a and the T_i/F_i bones (modelled as rigid bodies) have been considered in mutual contact at three points. The portion of each contact surface has been approximated by a spherical surface. More precisely, the areas of the surfaces of the mating bones which come into contact during the passive motion were digitized. Three contact points were selected and the corresponding contact areas (a cloud of digitized points for each area) approximated by their best fit spherical surfaces. The three contact points were identified at the inner area of the lateral malleolus and at the upper region of the distal T_i articulating with the top of the T_a surface, medially and laterally.

Experimental data confirmed [4] that fibers within CaFiL and TiCaL are nearly isometric during the ankle passive motion.

Based on these observations and assumptions a schematic of the ankle joint is shown in Figure 2.6a.

The two talocalcaneal and tibiofibular segments feature three sphere-to-sphere contact points being $\mathbf{A}_i$, and $\mathbf{B}_i$, $i = 3,4,5$, the centers of the mating spherical surfaces fixed to the Ta/Ca and Ti/Fi respectively. $\mathbf{A}_i$, and $\mathbf{B}_i$, $i = 1,2$ were the insertion points on the two segments of two isometric fibers of CaFiL and TiCaL respectively.

In this model the Ta/Ca segment has a one-DOF motion with respect to the Ti/Fi segment, considering that the rotations of the two fibers about the relevant longitudinal axis (defined by the attachment points $\mathbf{A}_1$, $\mathbf{B}_1$ for the former ligament and $\mathbf{A}_2$, $\mathbf{B}_2$ for the latter) are not essential to the relative pose of the two segments.

During the relative motion of the two segments, each pair of the mating spherical surfaces must maintain the contact, therefore the length $L_i = A_iB_i$, $i = 3,4,5$, is constant. Moreover, the length $L_i = A_iB_i$, $i = 1,2$ is also constant during passive motion since it represents the length of the ligament isometric fiber. As a conse-

quence, each pair of points ($\mathbf{A}_i$, $\mathbf{B}_i$), with $\mathbf{A}_i$ and $\mathbf{B}_i$, $i = 1,2,\ldots,5$, respectively fixed to the Ti/Fi and Ta/Ca segments, maintains a constant mutual distance during joint motion.

According to these assumptions, the equivalent mechanism is defined by two rigid bodies, i.e. the T_i/F_i and T_a/C_a segments, interconnected by five rigid binary links A_i and B_i, $i = 1,2,\ldots,5$ (Figure 2.6b). Here the meaning of the points $\mathbf{A}_i$, and $\mathbf{B}_i$, $i = 1,2,\ldots,5$, is the same as in Figure 2.6a. The elements $L_i = \mathbf{A}_i\mathbf{B}_i$, $i = 1,2,\ldots,5$, can be regarded as constant length rigid links connected to the base (T_i/F_i of Figure 2.6a) and to the movable link (platform, alias talocalcaneal link of Figure 2.6a) by spherical pairs centred at points $\mathbf{A}_i$ and $\mathbf{B}_i$, $i = 1,2,\ldots,5$, respectively. This mechanism is a fully-parallel mechanism of type 5-5 (five attaching points on the base and five on the platform) which provides the movable platform with one-DOF with respect to the base (rotation of links about the axes through their ending points $\mathbf{A}_i$ and $\mathbf{B}_i$, is irrelevant to the relative mobility of the two main segments). In the following considerations, for the sake of simplicity, the 5-5 fully-parallel mechanism will be renamed 5-5 FPM.

The closure equation of the 5-5 FPM that relates the independent variable of motion with the configuration of the mechanism can be found considering that each pair of points ($\mathbf{A}_i$, $\mathbf{B}_i$), $i = 1,2,\ldots,5$, are constrained to maintain a constant mutual distance, L_i, during motion. The closure equations of the equivalent mechanism of the ankle can then be expressed by:

$$\|\mathbf{A}_i - R\cdot\mathbf{B}_i - \mathbf{P}\| = L_i \qquad (i = 1,\ldots,5) \tag{2.11}$$

where the points $\mathbf{A}_i$ and $\mathbf{B}_i$ are measured in the reference systems S_f and S_c respectively. The symbol $\|\cdot\|$ is the L^2-norm of the vector, $\mathbf{P}$ is the position of the origin O_c of S_c in the reference system S_f and R is the rotation matrix as described in Section 2.2.1. The Cartesian reference systems S_f and S_c are embedded in the base and the platform respectively (see Figures 2.6a and 2.6b) and their locations are arbitrarily chosen.

The geometry of the equivalent 5-5 FPM is defined by 35 parameters: namely, $3\cdot 10 = 30$ coordinates of the centres of the spherical pairs and 5 link lengths L_i, $i = 1,2,\ldots,5$.

For a given geometry of the 5-5 FPM, equation system (2.11) can be regarded as a system of five nonlinear equations in six variables, i.e. the three components of vector $\mathbf{P}$ and the three orientation parameters α, β, and γ, which define the rotation matrix R. If, for instance, the ankle flexion angle γ is given, the remaining five variables can be obtained by solving the equation system (2.11). This nonlinear system is solved by means of a quasi-Newtonian numerical procedure. This problem is also known as direct position analysis of the mechanism. System (2.1) is a nonlinear system which normally provides more than one solution for a given value of the input angle γ [25]. Specific procedures could be used to find all the possible solutions [25], however, in this context only one solution is of practical interest and can be easily found by a numerical method, for instance, by a quasi-Newton numerical procedure [26], as explained in Section 3.2.

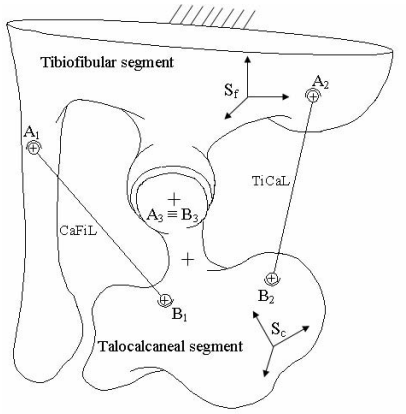

Figure 2.7: The spherical wrist mechanism applied to the ankle joint geometry.

2.3.2 The spherical wrist mechanism

Based on a careful inspection of the shape of the articular surfaces of the tibia/talus pair on one hand and on the experimental observation that the two ligaments TiCaL and CaFiL exhibit some isometric fibres during the passive motion, a one-DOF spherical wrist mechanism (SWM) was considered for the ankle passive motion simulation. The model of the mechanism is schematically shown in Figure 2.7 where the T_i and T_a surfaces are modelled as spherical surfaces (centred at $\mathbf{A}_3$ and $\mathbf{B}_3$) interconnected to each other to form a spherical pair centred at point $\mathbf{A}_3 \equiv \mathbf{B}_3$; the two isometric fibres $\mathbf{A}_1\mathbf{B}_1$ and $\mathbf{A}_2\mathbf{B}_2$ of the CaFiL and TiCaL ligaments respectively are modelled as two binary rigid links, with constant length L_i, $i = 1,2$, connected to the tibiofibular and to the talocalcaneal segments respectively by means of spherical pairs centered at points $\mathbf{A}_1$, $\mathbf{B}_1$ and $\mathbf{A}_2$, $\mathbf{B}_2$ respectively. A careful inspection reveals that the mechanism provides the T_a/C_a with one-DOF with respect to the T_i/F_i. Indeed, Kutzbach's formula [27] foresees one-DOF considering that the rotations of the two ligaments about the respective axes $\mathbf{A}_1\mathbf{B}_1$ and $\mathbf{A}_2\mathbf{B}_2$ are inessential to the relative position of the two segments.

The closure equations of the spherical wrist can be found based on the consideration that each pair of points ($\mathbf{A}_i$, $\mathbf{B}_i$), $i = 1,2$, is constrained to maintain a constant mutual distance L_i, during flexion motion while $\mathbf{A}_3$ and $\mathbf{B}_3$ must always be coincident. With these considerations, the model of the one-DOF spherical wrist can be expressed by:

$$\begin{aligned} &\|\mathbf{A}_i - R\cdot\mathbf{B}_i - \mathbf{P}\| = L_i \qquad (i = 1,2) \\ &\mathbf{A}_3 - R\cdot\mathbf{B}_3 - \mathbf{P} = 0 \end{aligned} \tag{2.12}$$

where the points $\mathbf{A}_i$ and $\mathbf{B}_i$ are expressed in the Cartesian reference systems S_f and S_c respectively and the symbol $\|\cdot\|$ is the L^2-norm of the vector. The systems S_f and S_c are embedded in the T_i/F_i and in the T_a/C_a respectively (Figure 2.7) and their

locations are arbitrarily chosen. The matrix R is the rotation matrix that transforms the components of a vector measured in S_c into the components of the same vector measured in the S_f and $\mathbf{P}$ is the position vector of the origin $\mathbf{O}_c$ of S_c with respect to the reference system S_f.

The equation system (2.12) represents the closure equation system of the one-DOF SWM. It is a system of five nonlinear equations in six variables: the three components of the position vector $\mathbf{P}$ and the three angles γ, α and β. Therefore, for every given angle γ, the remaining five variables can be found by solving the equation system (2.12).

The geometry of the equivalent spherical wrist is defined by 20 parameters: namely, the coordinates of points $\mathbf{O}_f$, $\mathbf{A}_1$, $\mathbf{A}_2$ in S_f and $\mathbf{O}_c$, $\mathbf{B}_1$, $\mathbf{B}_2$ in S_c and the 2 link lengths L_i, $i = 1,2$.

To solve efficiently the system 2.12, as described in Section 2.3.1, is possible to use a specific optimization procedure, will be explained in Section 3.2.

Chapter 3

Parameters optimization

In order to obtain the physical data necessary to synthesize the equivalent mechanisms proposed in the previous chapter, different experimental sessions were conducted. The results are then presented to show the accuracy of the models and the effectiveness of the proposed procedure.

3.1 In-vitro measurements

In order to evaluate the accuracy of the ankle models proposed in this dissertation, some experimental sessions were carried out at the Movement Analysis Laboratory of the Istituti Ortopedici Rizzoli (IOR), which provided also the experimental facilities and the indispensable surgical and technical assistance during the data acquisition.

In vitro experiments were carried out to measure anatomical geometry and passive motion at the human ankle complex. Passive motion was captured in-vitro in different specimens by means of a surgical navigation system with cluster of active markers attached to the T_i and T_a (Figure 3.1). The anatomical geometry of the passive structures, i.e. articular surfaces and attachment areas of the ligaments, were taken by digitisation with a pointer.

In particular, four skeleto-ligamentous lower leg preparations from lower limb amputation from four different subjects were analysed. Each specimen, including the intact T_i, F_i, T_a and C_a, was dissected at the Lisfranc joint line, free of all skin, subcutaneous and muscle tissues, leaving joint capsule, interosseous membrane and ligaments intact. A careful inspection of the specimens confirmed that they were not affected by deformations or arthritis. The T_i was fixed to an oblique arm at a horizontal workbench, with the toes upwards, whereas the other bones were left free to move [3, 16]. A pin drilled along the C_a longitudinal axis and protruding from the posterior surface came into contact with a rigid link, connected to the workbench by a revolute pair with axis parallel to the horizontal plane, which drove the pin to move with a five-DOF relative motion with respect to the link itself. An additional pin joined the T_a to the C_a, forcing the subtalar joint to have

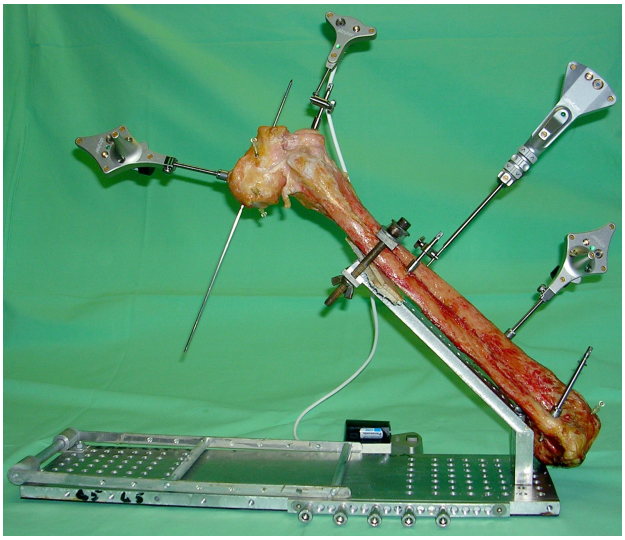

Figure 3.1: The experimental setting for the acquisition of the anatomical and kinematic data.

no relative motion. Starting from a rest position in maximum plantarflexion, the ankle was driven to dorsiflexion by moving the rigid link up and down, until maximum dorsiflexion, thus producing flexion at the T_a/C_a with respect to the T_i/F_i. Since the weight of the T_a/C_a and the friction between the pin and the rigid link are negligible, the motion of the T_a/C_a can be considered as in a virtually unloaded condition. An opto-electronic based motion tracking system[1] was used for recording the pose of the two trackers, fixed to T_i and T_a according only to rigidity of the fixation and visibility of the trackers by the cameras. The camera system collected the pose of the two trackers and of the pointer in a definite workspace. The pose of the trackers was measured with respect to a Cartesian reference system fixed to the camera system while the coordinates of points measured by the pointer are given in the reference system of the relevant tracker. The specimens were further dissected and both the geometry of the articular surfaces (Figure 3.2) and the insertion areas of the CaFiL and TiCaL ligaments were digitized by means of the same pointer.

3.2 The optimization procedure

In order to devise a models which targets best matching between models predictions and corresponding experimental measurements of the spatial motion, the physical relevance of the model can not be neglected. This means that the geometry (size and topology) of the mechanism was strictly related to the anatomical structures such as ligaments and bones of the ankle joint, which proved to be the

[1] Stryker Navigation System, Stryker, Kalamazoo, MI-USA; Freiburg/Breisgau-Germany

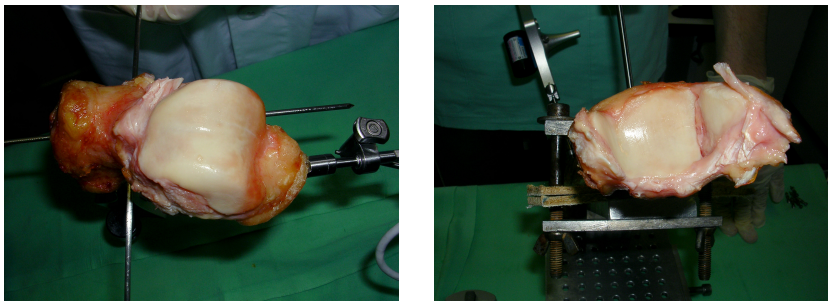

(a) (b)

Figure 3.2: Geometry of tibia and fibula surfaces (a) and talus surface (b) digitized by means of the pointer.

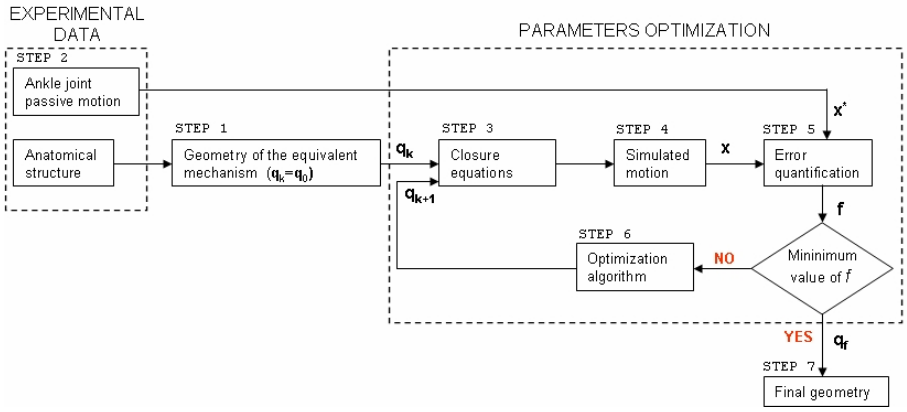

Figure 3.3: The optimization procedure.

main elements that guide the passive motion. This is an important point to relate the mathematical results of the model to the experimental ones, an aspect which becomes fundamental when the model is used for the study of the joint, for surgical purposes or for prosthetic design.

According this purpose an optimization procedure for the identification of the model parameters is presented. In particular, bounded optimization procedures make it possible to find the parameter set which reduces to a minimum the errors between the experimental and the simulated motions, at the same time keeping the parameter values sufficiently close to the anatomical observations. Starting from a first approximative solution deduced from the anatomical data, the final optimal geometry of the 5-5 FPM and SWM is obtained by means of an iterative refinement process.

The steps of the optimization procedure are presented in the following and the equivalent schema is shown in the Figure 3.3.

STEP 1. Based on some measurements of the main anatomical structures of the ankle, a first tentative geometry of the mechanism (5-5 FPM or SWM) is defined. A first approximation is required by the optimization procedure as a starting point for the numerical research of the optimum solution. The first approximation mechanism is based on the only experimental data but does not best-fit the anatomical passive motion. The parameters of the first mechanism are used also as a reference to define the domains of research, i.e. the bounds, for the optimization procedures.

STEP 2. A number n of measured relative positions and orientations (poses) of the talocalcaneal and tibiofibular segments are considered. This poses are collected during the experiment described in Section 3.1.

STEP 3. The matrix R defined in closure equation system is then evaluated for the n poses. The angles γ, α and β can then be computed from the elements of matrix R for the n poses.

STEP 4. The closure equation is solved for all n values of the flexion angle (γ), thus obtaining n sets of the five dependent variables.

STEP 5. In order to compare the pose of the platform with the pose obtained by measurement data, an error function f (objective function) is computed at each step of iteration. This function is the sum of the weighted errors of the experimental values with respect to the calculated values, for all n values of the flexion angle (γ). The function f is defined as follows:

$$f = \sum_{j=1}^{5} \sum_{i=1}^{n} \frac{\left(x_{ji} - x_{ji}^{*}\right)^2}{\left(x_{j_{max}} - x_{j_{min}}\right)^2} \tag{3.1}$$

where, x_{ji} is the actual value of the j-th dependent variable, $j = 1,2,\ldots,5$, at the i-th pose, $i = 1,2,\ldots,n$; x_{ji}^{*} is the corresponding experimental value of the variable x_{ji}; $x_{j_{max}}$ and $x_{j_{min}}$ are the maximum and minimum values of each of the dependent variables at the end of the process.

STEP 6. If equation system does not provide a real solution then the objective function f is given an arbitrarily high value. Therefore this solution is rejected and a new configuration is defined by the optimization algorithm (such as genetic algorithm).

STEP 7. If the objective function reaches a minimum the process stops, otherwise a new geometry of the 5-5 FPM is found and the iterative process is repeated.

Since the objective function is highly nonlinear and has discontinuities, the most traditional optimization methods, based on the gradient or on higher derivatives of the objective function and used to search for a relative minimum, do not provide good solutions to this problem. A different approach is therefore proposed. The optimization problem, that uses Eq. (3.1) as objective function, is

initially solved by means of a genetic algorithm or, alternatively, by means of the direct search method [28]; the obtained solution is then refined by means of a quasi-Newtonian algorithm [26].

It is worth introducing lower and upper bounds on the values of the parameters, so that the points that define the geometry of the equivalent mechanism provide a final geometry of the optimized equivalent mechanism which retains the anatomical feature of the ankle joint. This is particularly important if the synthesized model must be used for surgical preplanning or prosthesis design.

3.3 Results

The poses of the T_a with respect to the T_i obtained by the experimental sessions are compared with those obtained by both the SWM and the 5-5 equivalent FPM. The Figures shown in the following pages report both experimental and simulation data. In particular, the positions x, y, and z of the origin of the reference system S_c with respect to S_f and the angles α and β are reported as a functions of the ankle flexion angle γ.

The experimental results are identified by the symbol "Δ" and interpolated by a dash-dot line. The dash line and the continuous line represent the 5-5 FPM and the SWM respectively. The interpolation makes it possible to use a higher number of experimental data, which may be useful for the optimal synthesis of the geometry of both mechanisms (the 5-5 FPM and the SWM).

For the four specimens, the experimental passive motion compared very well with those obtained by the corresponding equivalent mechanisms. The Figures reveals that this was true for all 5 dependent variables, and therefore that the new equivalent spatial mechanisms were able to represent very well the passive motion of the human ankle joint.

For the 5-5 FPM the discrepancy on the positional variables was contained within about 2.5 mm; while the discrepancy on the rotational variables was lower than 1 degree for the internal/external rotation (α), and lower than 0.5 degrees for the pronation/supination (β). Furthermore, the degree of replication of the original passive joint motion was very high for each specimen. Indeed, in Table 3.1, for each specimen, the mean and the variance values over the full range of flexion angle γ of the difference between the final optimised simulation and the initial experimental data are reported.

The results of the 5-5 mechanism replicate the passive motion of the human ankle joint slightly better than those obtained by the one-DOF SWM. This is an expected result since the synthesis of the 5-5 FPM can rely upon a greater number of parameters and can thus better fit a more complex motion. However, although simpler and less capable of simulating a complex motion, the SWM represents a more useful basis for a reliable prosthetic design. Furthermore, the number of the SWM parameters being lower (fifteen) than those of the 5-5 FPM, the computational time during the optimization process is significantly reduced.

specimens		β	α	x	y	z
A	mean	0.095	0.370	0.192	0.373	0.448
	variance	0.016	0.238	0.058	0.163	0.267
B	mean	0.108	0.166	0.144	0.308	0.197
	variance	0.019	0.045	0.032	0.127	0.079
C	mean	0.455	0.488	1.078	0.254	1.538
	variance	0.297	0.374	2.144	0.082	3.819
D	mean	0.244	0.323	0.256	0.395	0.827
	variance	0.080	0.163	0.105	0.257	1.143

Table 3.1: Statistic data between the final optimised simulation and the initial experimental data; rotations are expressed in degrees, translations in millimeters.

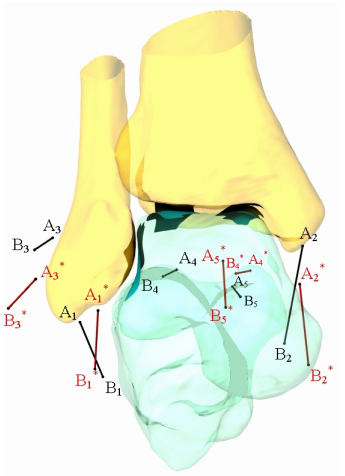

Figure 3.4: Initial (measured) and final (optimised) points $\mathbf{A}_i$, $\mathbf{B}_i$ and $\mathbf{A}_i^*$, $\mathbf{B}_i^*$ respectively, within the ankle complex joint in a typical specimen.

It is worth noting that different geometries of the equivalent 5-5 FPM and the SWM could have been synthesized, which might better fit the experimental data of the passive motion, but they might not better fit the anatomical structures of the natural ankle joint. The geometries synthesized in this dissertation are the best compromise that can well fit both the ankle passive motion and the ankle's main anatomical structures. Therefore, the geometrical parameters obtained from the optimisation process were also not far from the original values of the experimental measurements. For a typical specimen, a pictorial comparison between the initial tentative geometry of the 5-5 FPM and its synthesized final optimal geometry is reported in Figure 3.4 where points $\mathbf{A}_i$ and $\mathbf{B}_i$, $i = 1,2,\ldots,5$, are reported for the initial (black) and the final (red) geometry of the 5-5 FPM respectively.

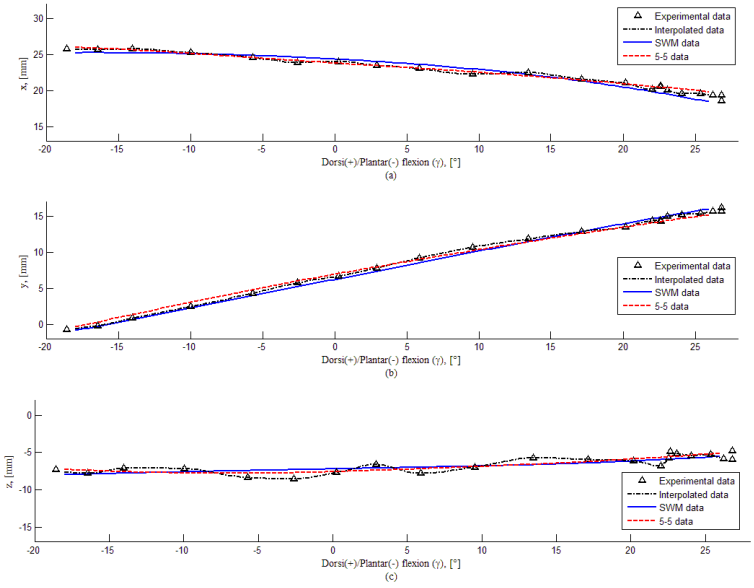

Figure 3.5: Passive motion simulation: x, (a), y, (b), and z, (c) versus ankle's flexion angle γ.

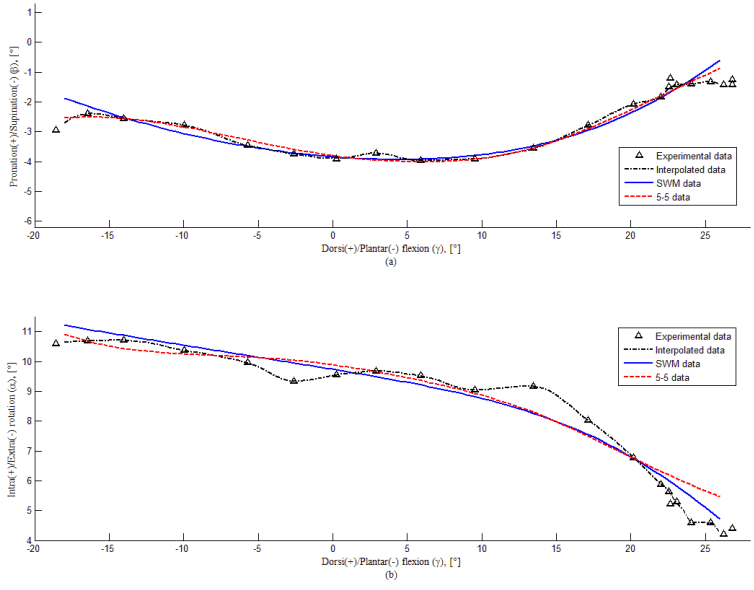

Figure 3.6: Passive motion simulation: angles β, (a), and α, (b), versus ankle's flexion angle γ.

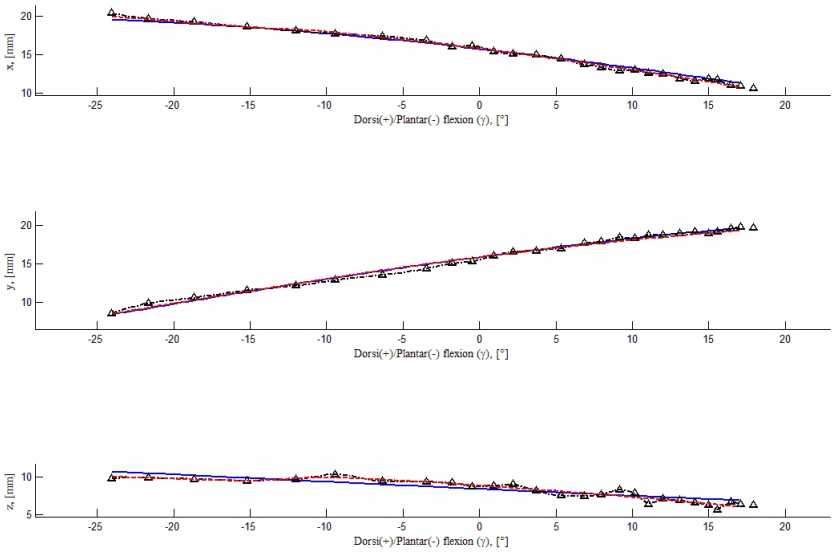

Figure 3.7: Passive motion simulation: x, (a), y, (b), and z, (c) versus ankle's flexion angle γ.

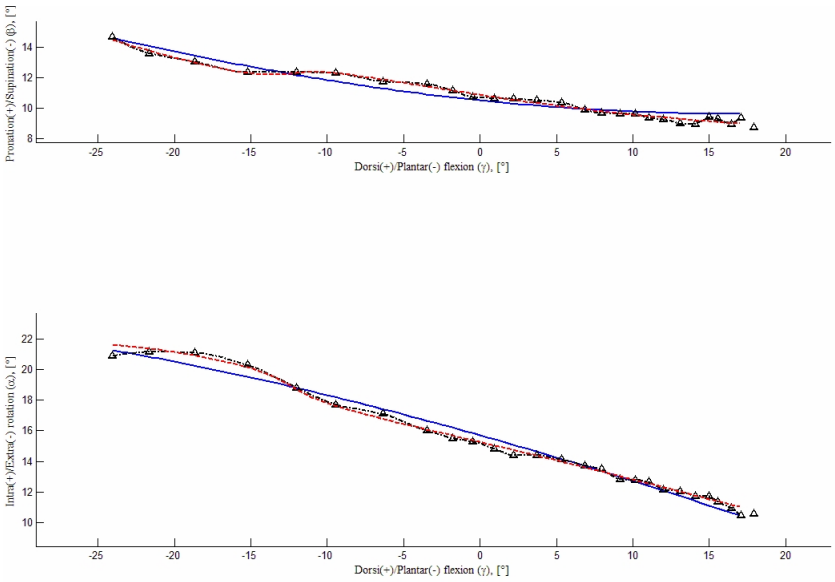

Figure 3.8: Passive motion simulation: angles β, (a), and α, (b), versus ankle's flexion angle γ.

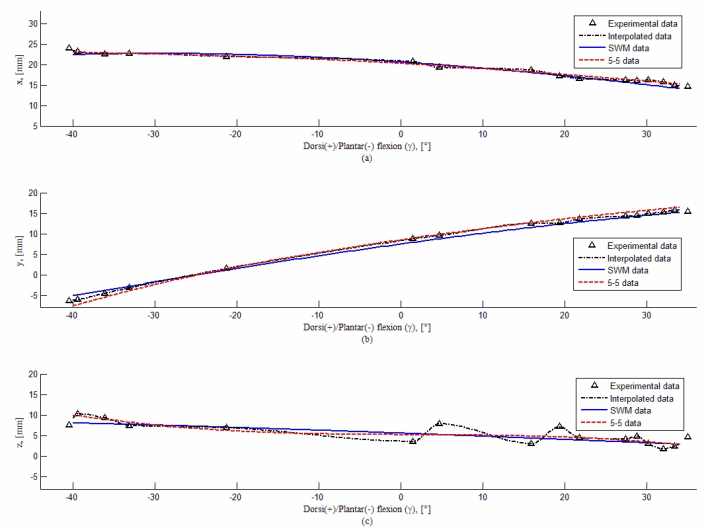

Figure 3.9: Passive motion simulation: x, (a), y, (b), and z, (c) versus ankle's flexion angle γ.

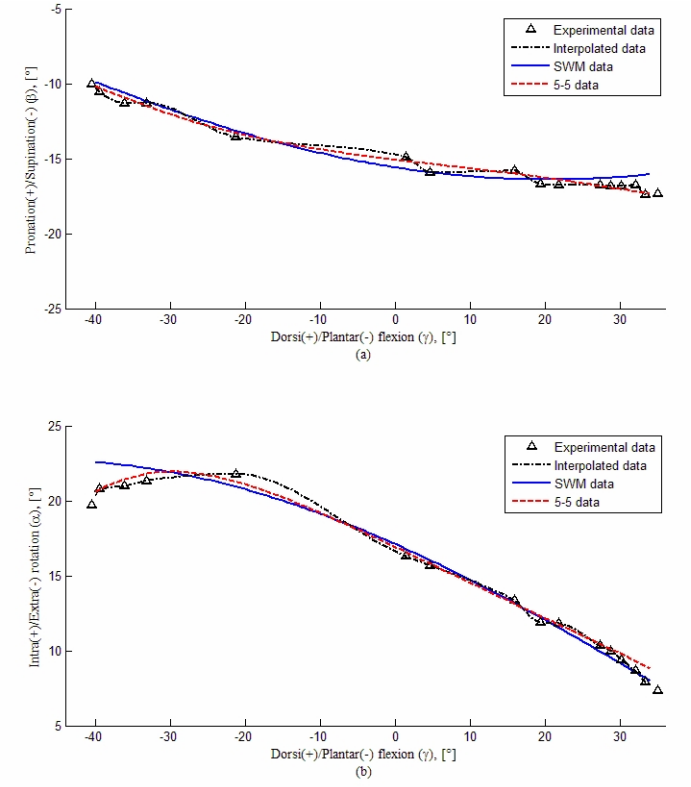

Figure 3.10: Passive motion simulation: angles β, (a), and α, (b), versus ankle's flexion angle γ.

Chapter 4

Conclusions

Designing spatial mechanisms for the simulation of passive motion at the human ankle joint complex can support effectively the development of functional-based prosthetic devices and ligament reconstruction techniques, including also rationale procedures for relevant computer-assisted pre-operative planning.

In this dissertation two one-DOF spatial equivalent mechanisms are presented for the simulation of the passive motion of the human ankle joint: the 5-5 fully parallel mechanism (5-5- FPM) and the fully parallel spherical wrist mechanism (SWM). These mechanisms are based on the main anatomical structures of the ankle joint, namely the talus/calcaneus and the tibio/fibula bones at their interface, and the TiCaL and CaFiL ligaments.

Some spatial equivalent mechanisms, based on the same anatomical structures, were presented in the literature [16]. Although in [16] it was shown the feasibility of the 3D modelling and the capacity of the proposed models to reproduce the original collected joint mobility, the comparison between the experimental results and the corresponding model predictions were not fully satisfactory. This was due to several oversimplifications, experimental and modelling limitations and to the use of a non optimal synthesis procedure.

In this dissertation, completely original data sets were collected in the present study and analysed by an innovative iterative procedure to synthesize the optimal geometry of the 5-5 FPM and SW.

The results of the 5-5 FPM replicate the passive motion of the human ankle joint considerably better than those obtained by the previous mechanisms. The 5-5 FPM is an effective tool for the study of both the human ankle motion and the role of its main anatomical structures. However, the geometrical complexity of the mechanism does not allow for an easy implementation in a practicable prosthetic design. In fact, a prosthesis design must combine both accuracy, to better replicate the kinematics of the limbs, and simplicity for an easy manufacturing. These features may be achieved by reducing the numbers of both links and kinematic pairs.

For this purpose, a one DOF spherical wrist mechanism (one-DOF SWM) is

proposed as an equivalent mechanism. Indeed, the SWM is geometrically simpler, although still accurate enough, and computationally less expensive than the 5-5 FPM and may also represent a better basis for the design of prosthetic devices. The simulation results compared with those of a one-DOF 5-5 parallel mechanism, which proved to simulate the ankle passive motion very well, exhibited a good degree of accuracy.

In conclusion, experimental results proved the efficiency of the proposed new mechanisms to simulate the ankle passive motion and, at the same time, the potentiality of the mechanism to replicate the ankle's main anatomical structures quite well. The new mechanisms represent a powerful tool for both pre-operation planning and new prosthesis design.

Bibliography

[1] T.P. Andriacchi, R.P. Mikosz, S.J. Hampton, and J.O. Galante. Model studies of the stiffness characteristics of the human knee joint. *Journal of Biomechanics*, 16:23–29, 1983.

[2] L. Blankevoort, R. Huiskes, and A. De Lange. Envelope of passive knee joint motion. *Journal of Biomechanics*, 21(9):705 – 720, 1988.

[3] A. Leardini, J.J. O'Connor, F. Catani, and S. Giannini. Kinematics of the human ankle complex in passive flexion: a single degree of freedom system. *Journal of Biomechanics*, 32(2):111–118, February 1999.

[4] A. Leardini, J.J. O'Connor, F. Catani, and S. Giannini. A geometric model of the human ankle joint. *Journal of Biomechanics*, 32(6):585–591, 1999.

[5] D.R. Wilson and J.J. O'Connor. A three-dimensional geometric model of the knee for the study of joint forces in gait. *Gait and Posture*, 5:108–115, 1997.

[6] J.R. Essinger, P.F. Leyvraz, Heegard J.H., and D.D. Robertson. Mathematical model for the evaluation of the behaviour during flexion of condylar-type knee prostheses. *Journal of Biomechanics*, 22(11-12):1229 – 1241, 1989.

[7] J.D. Goodfellows and J.J. O'Connor. The mechanics of the knee and prosthesis design. *Journal of Bone Joint Surgery*, 60B:358–369, 1978.

[8] J. Wismans, F. Velpaus, J. Janssen, A. Huson, and P. Struben. A three-dimensional mathematical model of the knee-joint. *Journal of Biomechanics*, 13:677685, 1980.

[9] E.A. Rahman and M.S. Hefzy. A two-dimensional dynamic anatomical model of the human knee joint. *ASME Journal of Biomechanical Engineering*, 115:357–365, 1993.

[10] T.S. Tumer and A.E. Engin. Three-body segment dynamic model of the human knee. *ASME Journal of Biomechanical Engineering*, 115:350–356, 1993.

[11] J.J. OConnor, T.L. Shercliff, E. Biden, and J.W. Goodfellow. The geometry of the knee in the sagittal plane. *Journal of engineering in Medicine*, 203:223–233, 1989.

[12] M.S. Hefzy and T.D.V. Cooke. Review of knee models: 1996 update. *Applied Mechanics Reviews*, 49(10 pt 2):187–193, 1996.

[13] V. Parenti-Castelli and R. Di Gregorio. Parallel mechanisms applied to the human knee passive motion simulation. In J. Lenarcic and M. Stanisic Eds., editors, *Advances in Robot Kinematics*, pages 333–344. Kluwer Academic Publisher, 2000. ISBN 0-7923-6426-0.

[14] R. Di Gregorio and V. Parenti-Castelli. A spatial mechanism with higher pairs for modelling the human knee joint. *Journal of Biomechanical Engineering*, 125(2):232 – 237, 2003.

[15] N. Sancisi and V. Parenti-Castelli. A 1-dof parallel spherical wrist for the modelling of the knee passive motion. In *Proceedings of the 12th IFToMM World Congress in Mechanism and Machine Science*, pages 1–6, June 2007.

[16] R. Di Gregorio, V. Parenti-Castelli, J.J. O'Connor, and A. Leardini. Mathematical models of passive motion at the human ankle joint by equivalent spatial parallel mechanisms. *Med Biol Eng Comput. 2007*, 45(3):305–313, 2007.

[17] Harold Ellis. *Gray's Anatomy: The Anatomical Basis of Medicine and Surgery*. Susan Standring, 39th edition (2004).

[18] A. Leardini, J.J. O'Connor, F. Catani F, and S. Giannini. The role of the passive structures in the mobility and stability of the human ankle joint: a literature review. *Foot Ankle Int*, 21(7):602–615, 2000.

[19] R. Stagni, A. Leardini, J.J. O'Connor, and S. Giannini. Role of passive structures in the mobility and stability of the human subtalar joint: a literature review. *Foot Ankle Int*, 24(5):402–409, 2003.

[20] Alberto Leardini, Rita Stagni, and John J. OConnor. Mobility of the subtalar joint in the intact ankle complex. *Journal of Biomechanics*, 34:805–809., 2001.

[21] A. Cappozzo, F. Catani, U.D. Croce, and A. Leardini. Position and orientation in space of bones during movement: anatomical frame definition and determination. *Clinical Biomechanics*, 10(4):171–178, 1995.

[22] E.S. Grood and W.J. Suntay. A joint coordinate system for the clinical description of three-dimensional motions: application to the knee. *Journal of Biomechanical Engineering*, 105(2):136–144, May 1983.

[23] R. Franci and V. Parenti-Castelli. A 5-5 one degree of freedom fully-parallel mechanism for the modelling of passive motion at the human ankle joint. In *Proceedings of ASME-IDETC/CIE 2007, International Design Engineering Technical Conferences and Computers and Information in Engineering*, pages 1–8, Las Vegas, Nevada, USA, September 2007.

[24] R. Franci and V. Parenti-Castelli. A one-degree-of-freedom spherical wrist for the modelling of passive motion of the human ankle joint. In A. Kecskemethy, editor, *Proceedings of IAK 2008, Conference on Interdisciplinary Applications of Kinematics*, pages 1–13, Lima, Peru, January 2008.

[25] C. Innocenti and V. Parenti-Castelli. Closed-form direct position analysis of a 5-5 parallel mechanism. *Journal of Mechanical Design, Transactions of the ASME*, 115(3):515–521, 1993.

[26] M.J.D. Powell. The convergence of variable metric methods for nonlinearly constrained optimization calculations. *Nonlinear Programming 3*, 3:27–63, 1978.

[27] K. Kutzbach. Mechanische leitungsverzweigung; ihre gesetze und anwendungen. *Maschinbau der Betrieb*, 8(21):710–716, 1929.

[28] V. Torczon. On the convergence of pattern search algorithms. *SIAM Journal on Optimization*, 7(1):1–25, 1997.